ANTIOXIDANTS & REDOX SIGNALING
Volume 25, Number 13, 2016

DOI: 10.1089/ars.2015.6562

FORUM ORIGINAL RESEARCH COMMUNICATION

mTORC2 Signaling Regulates Nox4-Induced Podocyte Depletion in Diabetes

Stéphanie Eid,[1,2] Suzan Boutary,[1] Kawthar Braych,[1] Ramzi Sabra,[3] Charbel Massaad,[2] Ahmed Hamdy,[4] Awad Rashid,[4] Sarah Moodad,[1] Karen Block,[5] Yves Gorin,[5] Hanna E. Abboud,[5] and Assaad A. Eid[1,*]

Abstract

Aim: Podocyte apoptosis is a critical mechanism for excessive loss of urinary albumin that eventuates in kidney fibrosis. Oxidative stress plays a critical role in hyperglycemia-induced glomerular injury. We explored the hypothesis that mammalian target of rapamycin complex 2 (mTORC2) mediates podocyte injury in diabetes. ***Results:*** High glucose (HG)-induced podocyte injury reflected by alterations in the slit diaphragm protein podocin and podocyte depletion/apoptosis. This was paralleled by activation of the Rictor/mTORC2/Akt pathway. HG also increased the levels of Nox4 and NADPH oxidase activity. Inhibition of mTORC2 using small interfering RNA (siRNA)-targeting Rictor *in vitro* decreased HG-induced Nox1 and Nox4, NADPH oxidase activity, restored podocin levels, and reduced podocyte depletion/apoptosis. Inhibition of mTORC2 had no effect on mammalian target of rapamycin complex 1 (mTORC1) activation, described by our group to be increased in diabetes, suggesting that the mTORC2 activation by HG could mediate podocyte injury independently of mTORC1. In isolated glomeruli of OVE26 mice, there was a similar activation of the Rictor/mTORC2/Akt signaling pathway with increase in Nox4 and NADPH oxidase activity. Inhibition of mTORC2 using antisense oligonucleotides targeting Rictor restored podocin levels, reduced podocyte depletion/apoptosis, and attenuated glomerular injury and albuminuria. ***Innovation:*** Our data provide evidence for a novel function of mTORC2 in NADPH oxidase-derived reactive oxygen species generation and podocyte apoptosis that contributes to urinary albumin excretion in type 1 diabetes. ***Conclusion:*** mTORC2 and/or NADPH oxidase inhibition may represent a therapeutic modality for diabetic kidney disease. *Antioxid. Redox Signal.* 25, 703–719.

Keywords: diabetic nephropathy, reactive oxygen species, NADPH oxidases, mTORC2

Introduction

DIABETIC NEPHROPATHY (DN) is one of the most serious complications of diabetes worldwide, affecting up to 25% and 40% of all patients with type 1 and type 2 diabetes, respectively. DN is the leading cause of end-stage renal disease and cardiovascular morbidity and mortality. The risk factors and mechanisms that contribute to the onset and development of these complications are poorly defined. The earliest clinical manifestation of DN in humans is increased urinary albumin excretion, which progresses to clinical proteinuria, one of the most important prognostic risk factors for kidney disease progression (11). Glomerular injury in diabetes is characterized by hypertrophy, glomerular mesangial cell activation resulting in matrix accumulation, basement membrane thickening, podocyte depletion/loss, and decreased abundance and mislocalization of slit diaphragm proteins that result in breach of glomerular barrier function and proteinuria, and ultimately, loss of renal function (1, 18, 20, 23, 26, 27, 29, 30, 32, 34–36, 38, 39). Among the different characteristics of glomerular morphology, the decreased number of podocyte per glomerulus is the strongest predictor

[1]Department of Anatomy, Cell Biology and Physiological Sciences, Faculty of Medicine and Medical Center, American University of Beirut, Beirut, Lebanon.
[2]UMR-S 1124 INSERM, Paris Descartes University, Sorbonne Paris Cite University, Centre Interdisciplinaire Chimie Biology, Paris, France.
[3]Department of Pharmacology and Toxicology, Faculty of Medicine and Medical Center, American University of Beirut, Beirut, Lebanon.
[4]Department of Nephrology, Hamad Medical Corporation, Doha, Qatar.
[5]Department of Medicine, South Texas Veterans Healthcare System and the University of Texas Health Science Center, San Antonio, Texas.

Innovation

This study reveals that a novel-signaling pathway involved in diabetes induces kidney injury. Our observations indicate that in addition to metabolic control, mammalian target of rapamycin (mTOR) inhibitors and/or antioxidants against Nox1 and Nox4 may represent an adjunct therapy to reduce/reverse glomerular injury in type 1 diabetes. Our finding that Nox1 and Nox4 are downstream targets of mTOR complex 2 (mTORC2) suggests that mTORC2 inhibitors may be used as therapeutic agents that may prevent oxidant-mediated cell injury in diabetes and provide a new strategy for inhibiting the progression of chronic kidney diseases.

of progression of DN, through which the fewer remaining cells predict a rapid progression of the disease (44, 46). We have previously shown that podocyte number is altered in diabetes, however, the mechanism of podocyte depletion/loss and the key players leading to podocyte dysfunction remain poorly defined.

The mammalian target of rapamycin (mTOR) signaling cascade controls cellular growth, survival, and metabolism (56). mTOR, a serine/threonine protein kinase, exists in two complexes, mTOR complex 1 (mTORC1) or mTOR complex 2 (mTORC2), consisting of distinct sets of protein-binding partners (9, 48). mTORC1 with its essential components mTOR, mLST8, and rapamycin-sensitive adaptor protein of mTOR (Raptor) mediates protein synthesis and cell size (56) through p70S6 kinase (p70S6K)/S6 kinase 1 (S6K1) and 4E-binding protein 1 (4E-BP1) (23, 54). We have recently shown that podocyte apoptosis, induced by either type 1 diabetes *in-vivo* or by exposure to high-glucose (HG) concentrations *in-vitro*, was mediated by activation of the mTORC1 pathway through inactivation of the AMPK/tuberin pathway (16). We further demonstrated that the activation of mTORC1 enhanced oxidative stress *via* upregulation of Nox1 and Nox4 expression and NADPH oxidase activity (16–18). Nox2 expression appeared to be unchanged in podocytes exposed to HG, or in glomeruli isolated from type 1 diabetic mice (18). Inhibition of the mTOR pathway using rapamycin significantly reversed the observed changes. Furthermore, the inhibition of mTOR with rapamycin significantly decreased glomerular epithelial cell apoptosis, reduced glomerular basement membrane (GBM) thickening and foot process effacement, and attenuated mesangial expansion and albuminuria (16).

In contrast to mTORC1, very little is known regarding the potential function of mTORC2 in glomerular maintenance and disease and the current data are controversial (26, 30, 47, 50, 52). The rapamycin-insensitive complex (mTORC2) comprises mTOR, mSIN1, mLST8, and the rapamycin-insensitive subunit Rictor. mTORC2 phosphorylates protein kinase B (PKB/Akt) at Ser473 (50) and has been implicated in controlling cell survival and cytoskeletal organization (56). In this study, we show that in type 1 diabetes, or in cells exposed to HG, podocytes undergo apoptosis that is mediated by the activation of the Rictor/mTORC2 pathway. We also demonstrate that in type 1 diabetic mice, the activation of Rictor/mTORC2 enhances oxidative stress production *via* upregulation of Nox4 expression and NADPH oxidase activity. Inhibition of the Rictor/mTORC2 pathway reverses the effect of HG-induced reactive oxygen species (ROS) production by decreasing Nox4 messenger RNA (mRNA) levels, protein expression, and NADPH oxidase activity. More importantly, we show that inhibition of Rictor/mTORC2 decreases podocyte depletion, reduces GBM thickening and foot process effacement, and attenuates albuminuria.

Results

HG regulates the signaling activation of the Rictor/mTORC2 pathway in podocytes

Exposure of mouse podocytes to 25 m*M* glucose (HG) resulted in a relatively rapid increase in Rictor mRNA levels and protein levels, compared with cells incubated in 5 m*M* glucose (normal glucose) or 25 m*M* of mannitol used as osmotic control (Fig. 1A, D). Rictor activation was accompanied by an increase in the phosphorylation of its downstream target Akt^{Ser473} (Fig. 1E) and an increase in the phosphorylation of $NDRG1^{Thr346}$, used as a measure of mTORC2 activity (Fig. 1G). Dual phosphorylation on Thr308 and Ser473 is required for the activation of Akt. Our results showed that exposure of podocyte to HG also significantly increased the phosphorylation of Akt^{Thr308} (Fig. 1F). These findings were associated with an increase in Akt1 and Akt2 mRNA levels and protein expression (Fig. 1B, C, E, H, I).

Rictor/mTORC2 signaling activation mediates HG-induced podocyte injury

We have previously shown that HG induces podocyte injury by altering slit diaphragm proteins, podocin, and by inducing podocyte depletion (16–18). We next examined whether mTORC2 mediates the effect of HG-induced podocyte injury. Mouse podocytes were transfected with SMART pool of siRictor or with nontargeting small interfering RNA (siRNA) (Scr) before exposure to HG for 48 h. Glucose treatment was associated with a decrease in podocin protein expression and an increase in podocyte apoptosis as assessed by annexin V binding, caspase 3 activation, and cellular DNA fragmentation (Fig. 2A–D). These results were paralleled by an increase in Rictor mRNA levels and protein expression, an increase in the phosphorylation of Akt^{Ser473} and $NDRG1^{Thr346}$ (Fig. 2E, I, M), and an increase in the mRNA levels and protein expression of Akt1 and Akt2 (Fig. 2F, G, K, L). In this set of experiments, phosphorylation of Akt^{Thr308} was also increased (Fig. 2J). We have previously shown that in podocytes treated with HG, the mTORC1/p70S6 kinase pathway was activated (16). As expected, in this set of experiments, the mTORC1 pathway determined by the increase in Raptor and in p70-S6K phosphorylation on Thr389 was activated (Fig. 2N, O). Transfection of mouse podocytes with SMART pool of siRictor or with nontargeting siRNA (Scr) before exposure to HG for 48 h decreased Rictor mRNA levels and protein expression (Fig. 2E, H), reversed HG-induced Akt phosphorylation on Ser 473 and NDRG1 phosphorylation on Thr346 (Fig. 2I, M), and decreased Akt1and Akt2 mRNA levels and protein expression (Fig. 2F, G, K, L). The use of siRictor also inhibited HG-induced podocyte injury measured by podocin alteration and podocyte apoptosis (Fig. 2A–D). On the contrary, siRictor treatment did not influence the effect of HG on Raptor protein expression (Fig. 2N) or on the phosphorylation of Akt^{Thr308} and $p70S6K^{Thr389}$ (Fig. 2J, O). Furthermore, siRaptor did

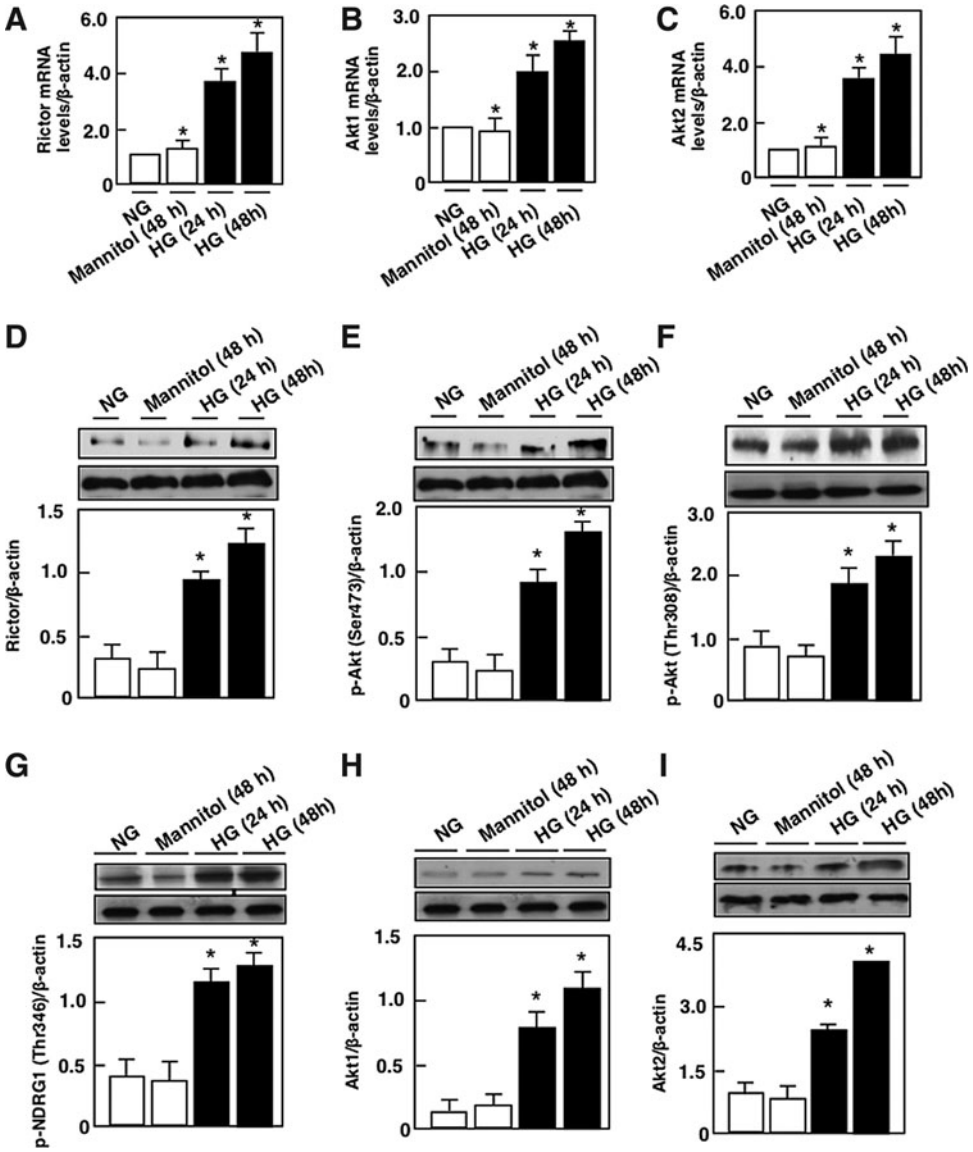

FIG. 1. Effect of HG on the Rictor/mTORC2 pathway. Mouse podocytes were exposed to either HG (25 m*M*) or NG (5 m*M*) for 24 or 48 h. Twenty-five millimolars of mannitol was used as osmotic control. Relative mRNA amount of **(A)** Rictor, **(B)** Akt1, and **C)** Akt2. **(D)** Histograms showing quantitation of Rictor/*β*-actin. **(E)** Histograms showing quantitation of p-Akt (Ser473)/*β*-actin. **(F)** Histograms showing quantitation of p-Akt (Thr308)/*β*-actin. **(G)** Histograms showing quantitation of p-NDRG1 (Thr346)/*β*-actin. **(H)** Histograms showing quantitation of Akt1/*β*-actin. **(I)** Histograms showing quantitation of Akt2/*β*-actin. All values are the mean ± SE from four independent experiments ($n=4$). *$p<0.05$ *versus* control. Akt, protein kinase B; HG, high glucose; mRNA, messenger RNA; mTORC2, mammalian target of rapamycin complex 2; NG, normal glucose; SE, standard error.

not alter HG-increased Rictor mRNA levels and protein expression nor the phosphorylation of Akt on Ser473 (Supplementary Fig. S1A–C; Supplementary Data are available online at www.liebertpub.com/ars). Collectively, these results indicate that mTORC2 activation by HG mediates podocyte injury, independently from the mTORC1 pathway.

To study if mTORC1 and mTORC2 have an additive effect on podocyte injury, we used an ATP competitive inhibitor of mTOR, the PP242, known to block both kinase complexes (10). PP242 in culture had the same effect on mTORC inhibition as inhibition of both TORC1 and TORC2 simultaneously by downregulating Raptor and Rictor, using two independent small hairpin RNAs (shRNAs) (10). In this study, therefore, blockade of mTORC1 and mTORC2 by PP242 reversed HG-induced podocyte injury (Fig. 3A–D), such that the percentage of apoptotic cells assessed by annexin V and cellular DNA fragmentation returned to levels similar to control with the use of PP242; in contrast, the blockade of mTORC2 alone reversed apoptosis only partially, although significantly (Fig. 2B, D). In previous studies, we provided evidence that hyperglycemia/HG-induced podocyte apoptosis was mediated by activation of the mTORC1 pathway through inactivation of AMPK (16). In this study, we showed that mTORC2 inactivation partially, but not significantly, reversed HG-induced AMPK inactivation (Supplementary Fig. S2). Taken together, these results may suggest that the activations of mTORC1 and mTORC2 are independent processes in diabetes-induced podocyte injury, and that these two pathways may have an additive or synergistic effect on the reversal of the injury.

Rictor/mTORC2 regulates HG-induced ROS production, NADPH oxidase activity, Nox1 and Nox4 mRNA and protein levels

Nox4 is known to be constitutively active and the upregulation of its protein levels directly accounts for the increased NADPH-dependent superoxide production (28). Several studies have shown that Nox4 generates superoxide (28), especially those performed in vascular smooth cells, and in cardiac or renal cells and tissue (4, 7, 8, 17, 18, 28, 29). In those studies, superoxide production was measured by high

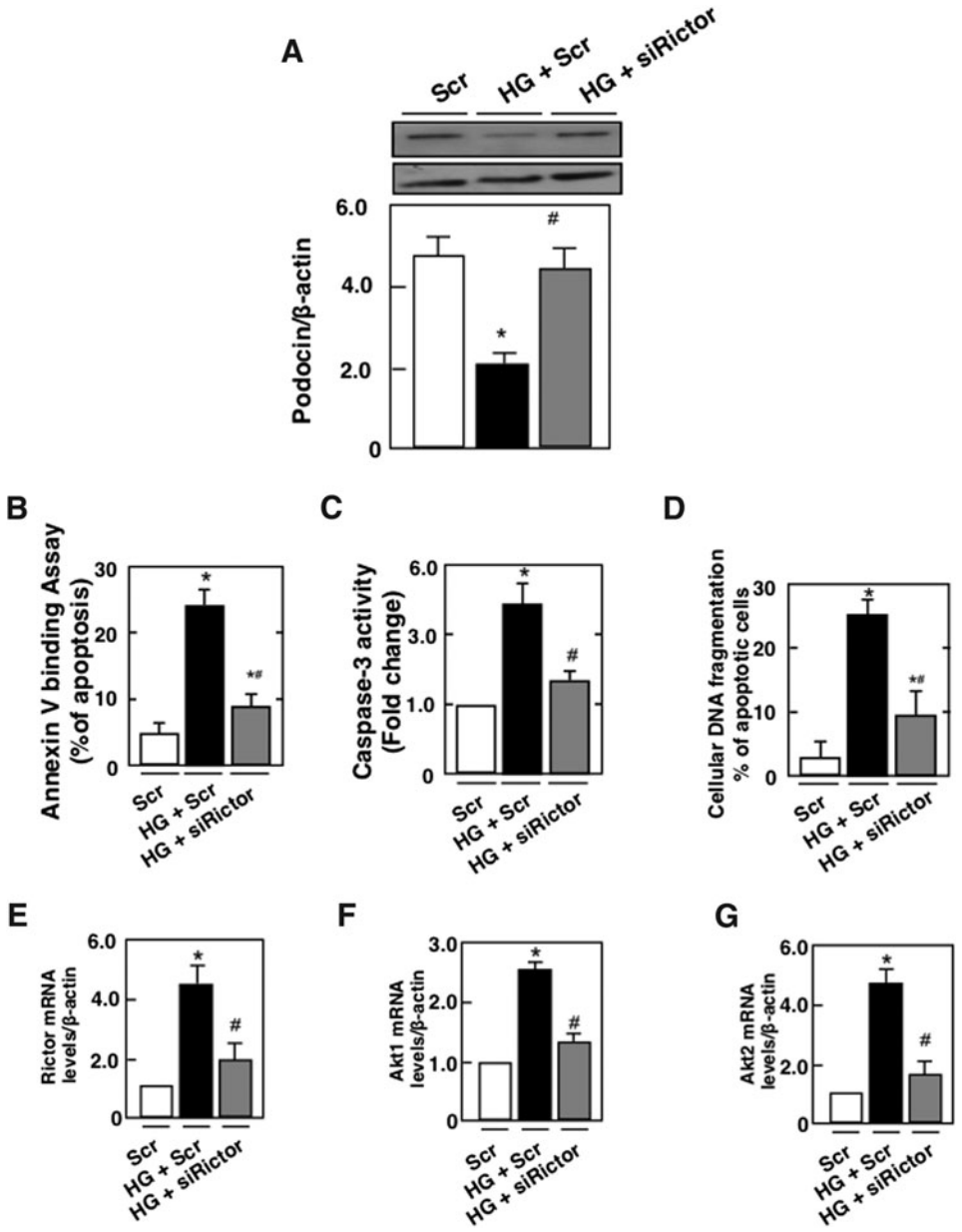

FIG. 2. HG induces podocyte apoptosis through activation of the Rictor/mTORC2 signaling pathway. Mouse podocytes were transfected with scrambled siRNA (nontargeting; Scr) or with siRNA for Rictor (siRictor) in NG or HG. Podocytes were incubated with NG or HG for 48 h after transfection. Treatment with siRictor but not Scr inhibited HG-induced podocyte injury. **(A)** Histograms showing quantitation of Podocin/β-actin. Podocyte apoptosis was assessed by **(B)** annexin V binding, **(C)** caspase 3 activity, and **(D)** cellular DNA fragmentation. Podocyte injury was accompanied by activation of the Rictor/mTORC2 pathway. **(E)** Relative mRNA levels of Rictor in control and treated podocytes after transfection. **(F)** Relative mRNA levels of Akt1 in control and treated podocytes after transfection. **(G)** Relative mRNA levels of Akt2 in control and treated podocytes after transfection. **(H)** Histograms showing quantitation of Rictor/β-actin. **(I)** Histograms showing quantitation of p-Akt (Ser473)/β-actin. **(J)** Histograms showing quantitation of p-Akt (Thr308)/β-actin. **(K)** Histograms showing quantitation of Akt1/β-actin. **(L)** Histograms showing quantitation of Akt2/β-actin. **(M)** Histograms showing quantitation of p-NDRG1 (Thr346)/β-actin. **(N)** Histograms showing quantitation of Raptor/β-actin. **(O)** Histograms showing quantitation of p-p70S6K^{Thr389}/p70S6K. All values are the mean ± SE from four independent experiments ($n = 4$). $^{*}p < 0.05$ *versus* control; $^{\#}p < 0.05$ *versus* HG. p70S6K, 70-kDa ribosomal protein S6 kinase; siRNA, small interfering RNA.

performance liquid chromatography (HPLC) analysis of 2-hydroxyethidium (EOH), the dihydroethidium (DHE)-derived oxidation product specific for superoxide, or electron paramagnetic/spin resonance, lately acknowledged to be two ''gold standard techniques'' for superoxide measurement (7, 13, 28). Beside the vasculature or the kidney, Nox4-mediated superoxide production was detected in other systems (28, 33, 41). We have previously shown that NADPH oxidase Nox4 plays an important role in podocyte injury (16–19).

To establish that Nox4 is necessary for HG-induced ROS production, Nox4 expression was downregulated with specific siRNAs. Transfection with siNox4, but not with Scr,

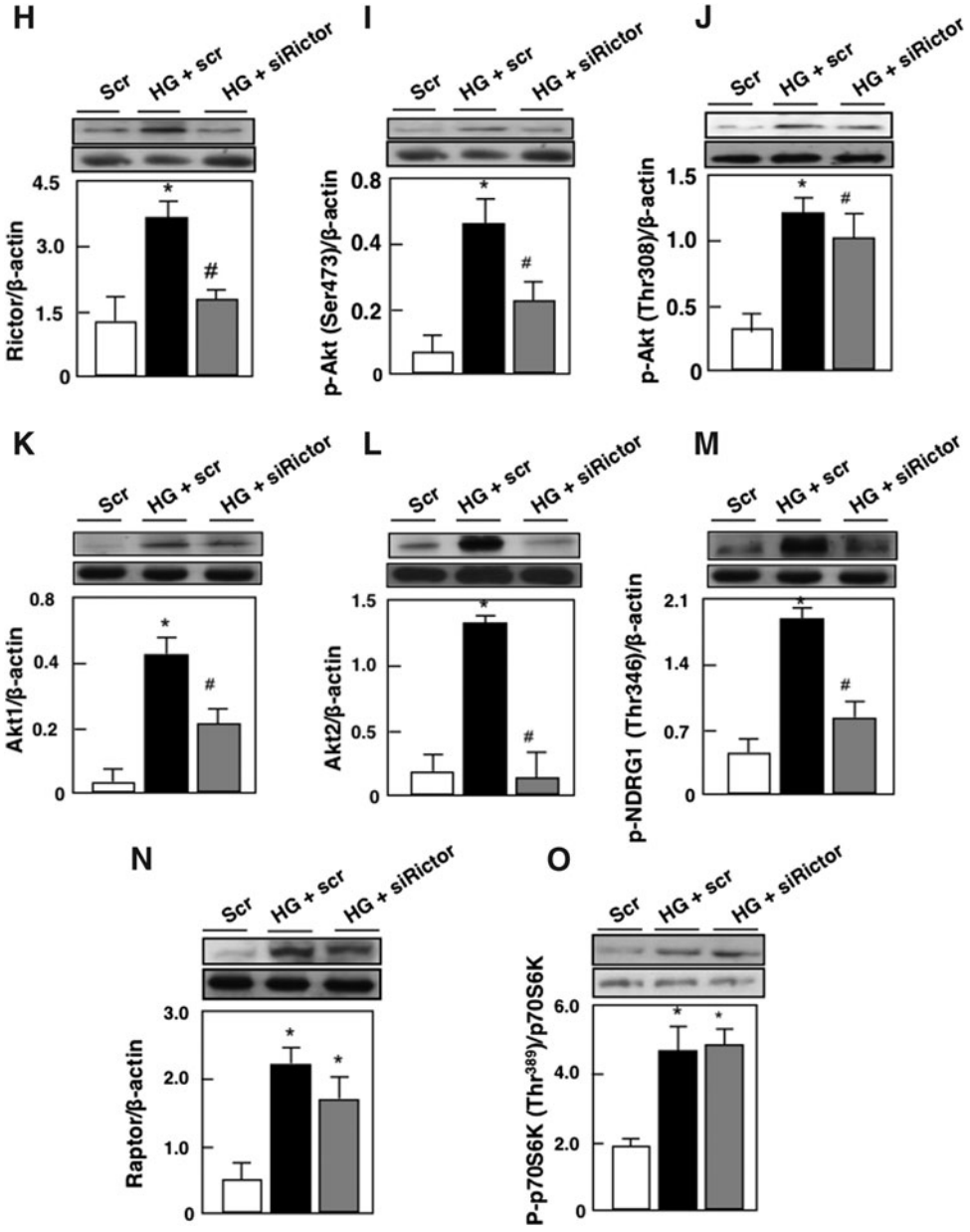

FIG. 2. (continued).

reduced Nox4 protein abundance (Supplementary Fig. S3A, B). Furthermore, siNox4 nearly abrogated the HG-induced NADPH oxidase activity (Supplementary Fig. S3C) and intracellular superoxide generation (Supplementary Fig. S3D). Like Nox4, the primary biochemical function of Nox1 is superoxide production, which is then converted to H_2O_2. With respect to Nox1, this isoform appears to play a major role in diabetic macrovascular diseases but not much is known about the role of Nox1 in DN (31, 37). To assess whether mTORC2 regulates ROS production and NADPH oxidase Nox1 and Nox4, podocytes were transfected with siRictor and incubated with HG. mTORC2 inactivation reversed HG-induced ROS production (Fig. 4A), Nox1 and 4 mRNA (Fig. 4B, C), and protein expression (Fig. 4D, E) and significantly blocked HG-induced NADPH oxidase activity (Fig. 4F) and superoxide production (Fig. 4F). Taken together, our data suggest that HG increases ROS production, Nox1 and Nox4 mRNA levels, and protein expression, and that activation of the NADPH oxidase is mediated, at least partially, through a Rictor/mTORC2-dependent mechanism.

Rictor/mTORC2 pathway is activated in glomeruli in type 1 diabetes

The effect of mTORC2 blockade by antisense (AS) oligonucleotide targeting Rictor treatment was studied in OVE26 mice, a model of type 1 diabetes. The FVB-OVE26 mouse (JAX No. 5564; The Jackson Laboratory, Bar Harbor, ME) is a transgenic model of early-onset type 1 diabetes, generated directly onto the FVB/N background. These mice develop diabetes within the first weeks of life as a result of β-cell toxicity in response to calmodulin gene overexpression.

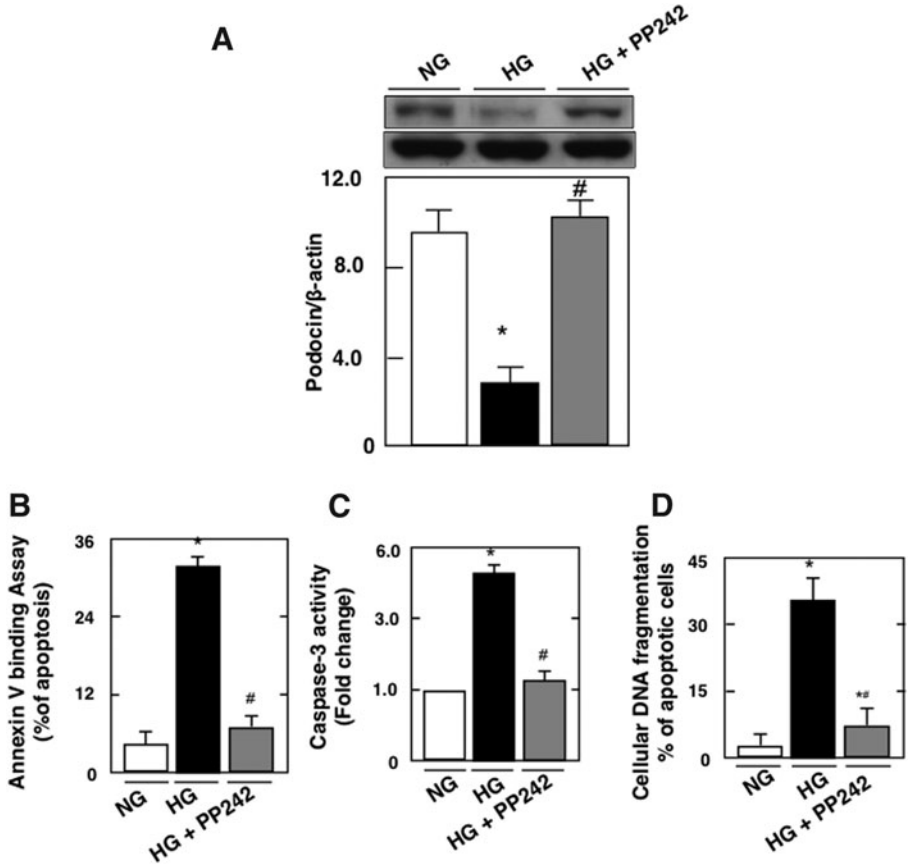

FIG. 3. Total inhibition of the mTORC pathway restored the integrity of the podocytes. Mouse podocytes were pretreated with 1 μM of PP242. After 1 h, cells were exposed to HG in the presence or absence of the inhibitor for 48 h. Treatment with PP242 reversed podocyte injury and restored the integrity of the podocytes. **(A)** Histograms showing quantitation of Podocin/β-actin. Podocyte apoptosis was assessed by **(B)** annexin V binding, **(C)** caspase 3 activity, and **(D)** cellular DNA fragmentation. All values are the mean ± SE from four independent experiments ($n = 4$). $^{*}p < 0.05$ *versus* control; $^{\#}p < 0.05$ *versus* HG.

The OVE26 mice live and maintain their body weights well over 1 year with no insulin treatment. These mice show a progressive increase in their urine albumin levels exceeding 15,000 μg/24 h at 9 months of age paralleled by a decrease in their glomerular filtration rate. In conjunction, they develop progressively enlarged glomeruli, an enlarging mesangium with diffuse and nodular expansion of mesangial matrix, tubulointerstitial fibrosis, and thickening of the GBM (2, 57). In this study, OVE26 mice were treated with phosphorothioate sense (S) or (AS) oligonucleotides targeting Rictor (90 ng·g body wt^{-1}·day^{-1} for 5 weeks), administered subcutaneously by an ALZET osmotic minipump (Alza, Palo Alto, CA). Control FVB mice were treated with vehicle (19). Because of their nuclease stability and relative ease of synthesis, the phosphorothioates are the most widely studied oligonucleotides; they are highly soluble and have excellent AS activity (12). OVE26 mice had elevated blood glucose levels compared with FVB mice and were not affected by S or AS treatment (Table 1). Body weight was significantly reduced in the OVE26 mice compared with FVB littermates. Total kidney weight and kidney-to-body weight ratio, indices of renal hypertrophy, increased significantly in OVE26 mice compared with control FVB mice. Kidney size in OVE26 mice treated with AS was significantly reduced compared with nontreated OVE26 mice or OVE26 treated with S (Table 1). Urine flow rate (UFR) was increased in OVE26 mice compared with FVB mice, and S or AS treatment had no effect on UFR (Table 1). In isolated glomeruli from the two kidneys of each mice, Rictor mRNA levels and protein expression were significantly increased in OVE26 compared with FVB (Fig. 5A, D, E). Akt1 and Akt2 mRNA levels and protein expression as well as phosphorylated Akt^{Ser374} and NDRG1^{Thr346} were also increased in OVE26 compared with FVB control littermates (Fig. 5B–D, F, H–J), indicating activation of the Rictor/mTORC2 pathway. Akt phosphorylation on Thr308 was also increased in the OVE26 mice compared with FVB (Fig. 5D, G). In parallel, raptor protein expression and phosphorylated p70 S6K^{Thr389} were increased in the isolated glomeruli of OVE26 compared with FVB (Fig. 5K–M), indicating activation of mTORC1 kinase. Treatment with AS decreased Rictor mRNA levels and protein expression (Fig. 5A, D, E), as well as mRNA levels and protein expression of Akt1 and Akt2 (Fig. 5B–D, I, J) concomitant with a decrease in Akt phosphorylation on Ser374 and NDRG1 phosphorylation on Thr346 (Fig. 5D, F, H), but had no effect on Raptor nor on the phosphorylation of p70 S6K^{Thr389} (Fig. 5K–M). Taken together, our data show that AS treatment significantly reduced mRNA levels and protein expression of Rictor by almost 60%–70% and decreased the phosphorylation of its downstream effector the Akt^{Ser374} and the phosphorylation of NDRG1 on Thr346 but had no effect on the mTORC1 activation, confirming the *in vitro* observation that mTORC2 acts independently of mTORC1 in our model. In all these experiments, sense oligonucleotides targeting Rictor did not alter the effect of hyperglycemia on the observed changes in the isolated glomerulus of the OVE26 type 1 diabetic mice (Table 1).

Rictor/mTORC2 activation upregulates Nox4 and enhances NADPH oxidase activity in type 1 diabetes

We next examined the relationship between NADPH oxidase Nox4 as the major NADPH oxidase in the kidney and

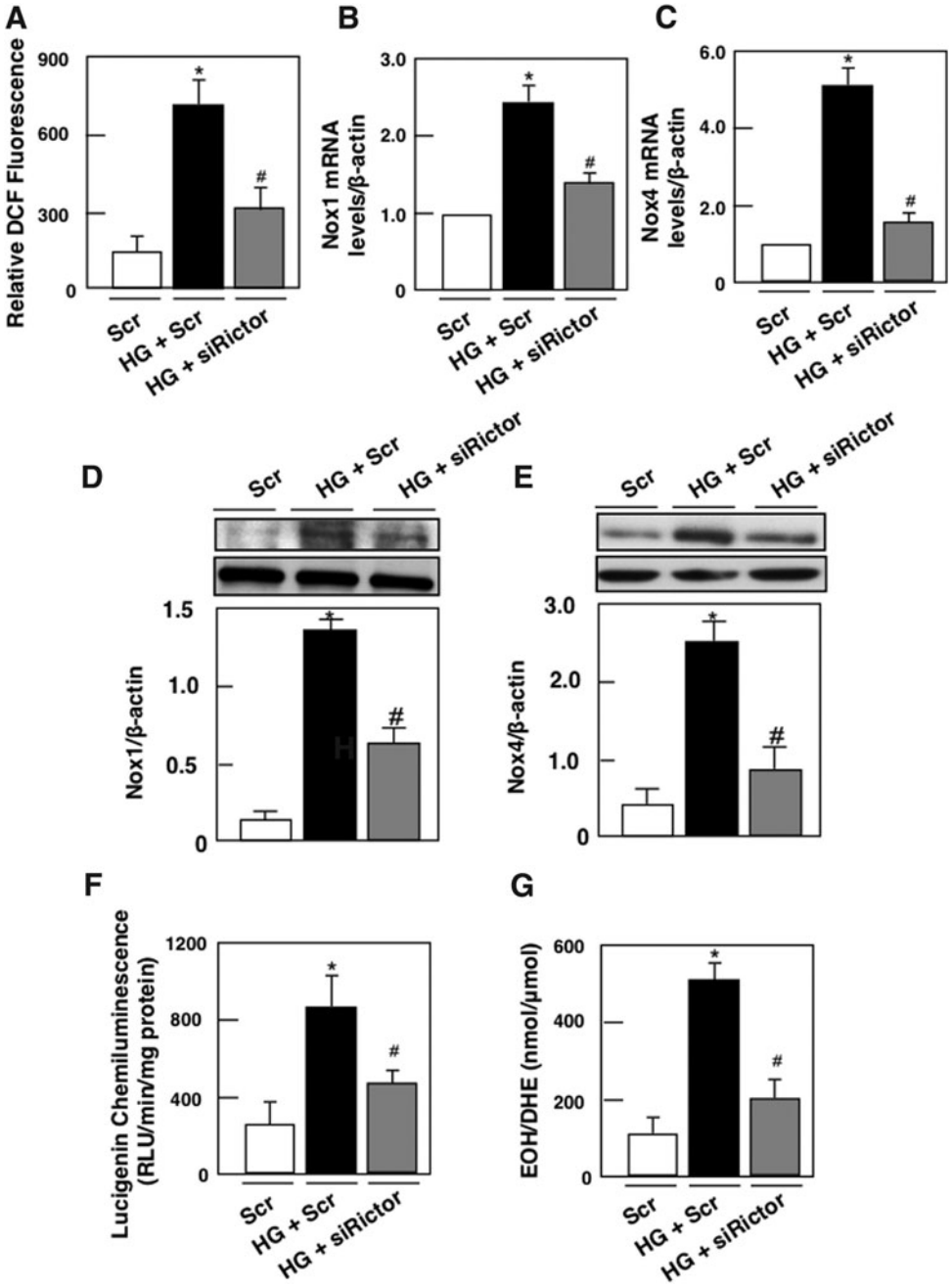

FIG. 4. Rictor/mTORC2 signaling pathway regulates HG-induced ROS production, Nox1 and Nox4 mRNA and protein levels, NADPH oxidase activity, and superoxide production. Mouse podocytes were transfected with scrambled siRNA (nontargeting; Scr) or with siRNA for Rictor (siRictor) in NG or HG. Podocyte were incubated with NG or HG for 48 h after transfection. **(A)** ROS generation measured by DCF with a multiwell fluorescence plate reader. **(B)** Relative mRNA levels of Nox1. **(C)** Relative mRNA levels of Nox4. **(D)** Histograms showing quantitation of Nox1/β-actin from four different experiments ($n=4$). **(E)** Histograms showing quantitation of Nox4/β-actin from four different experiments ($n=4$). **(F)** NADPH-dependent superoxide generation. **(G)** Superoxide generation evaluated using DHE and HPLC. All values are the mean ± SE from four independent experiments. $^{*}p<0.05$ *versus* control; $^{\#}p<0.05$ *versus* HG. DHE, dihydroethidium; HPLC, high performance liquid chromatography; ROS, reactive oxygen species.

TABLE 1. GLUCOSE LEVEL, BODY WEIGHT, KIDNEY WEIGHT, KIDNEY WEIGHT TO BODY WEIGHT RATIO, AND URINE FLOW RATE OF FVB CONTROL MICE, OVE26 TYPE 1 DIABETIC MICE, AND OVE26 MICE TREATED WITH SENSE OR ANTISENSE OLIGONUCLEOTIDES TARGETING RICTOR

	Control FVB	*Diabetic OVE26*	*Diabetic OVE26+sense Rictor*	*Diabetic OVE26+antisense Rictor*
Glucose level (m*M*)	145 ± 10	495 ± 10[a]	480 ± 15[a]	485 ± 18[a]
Body weight (g)	26 ± 1.4	18.5 ± 1.3[a]	19.5 ± 1.5[a]	20 ± 1.5[a]
Kidney weight (g)	0.20 ± 0.02	0.28 ± 0.04[a]	0.25 ± 0.02[a]	0.18 ± 0.07[b]
Kidney weight/body weight (g/kg)	8.1 ± 0.7	15.3 ± 0.9[a]	13.5 ± 0.6[a]	9.3 ± 0.4[b]
Urine flow rate (ml/24 h)	0.7 ± 0.04	8.5 ± 0.7[a]	8.0 ± 0.5[a]	8.5 ± 0.5[a]

Values are mean ± standard error from 10 animals for each group ($n=10$).
[a]$P<0.05$ or 0.001 *versus* FVB mice; [b]$P<0.05$ or 0.001 *versus* diabetic OVE26 mice.

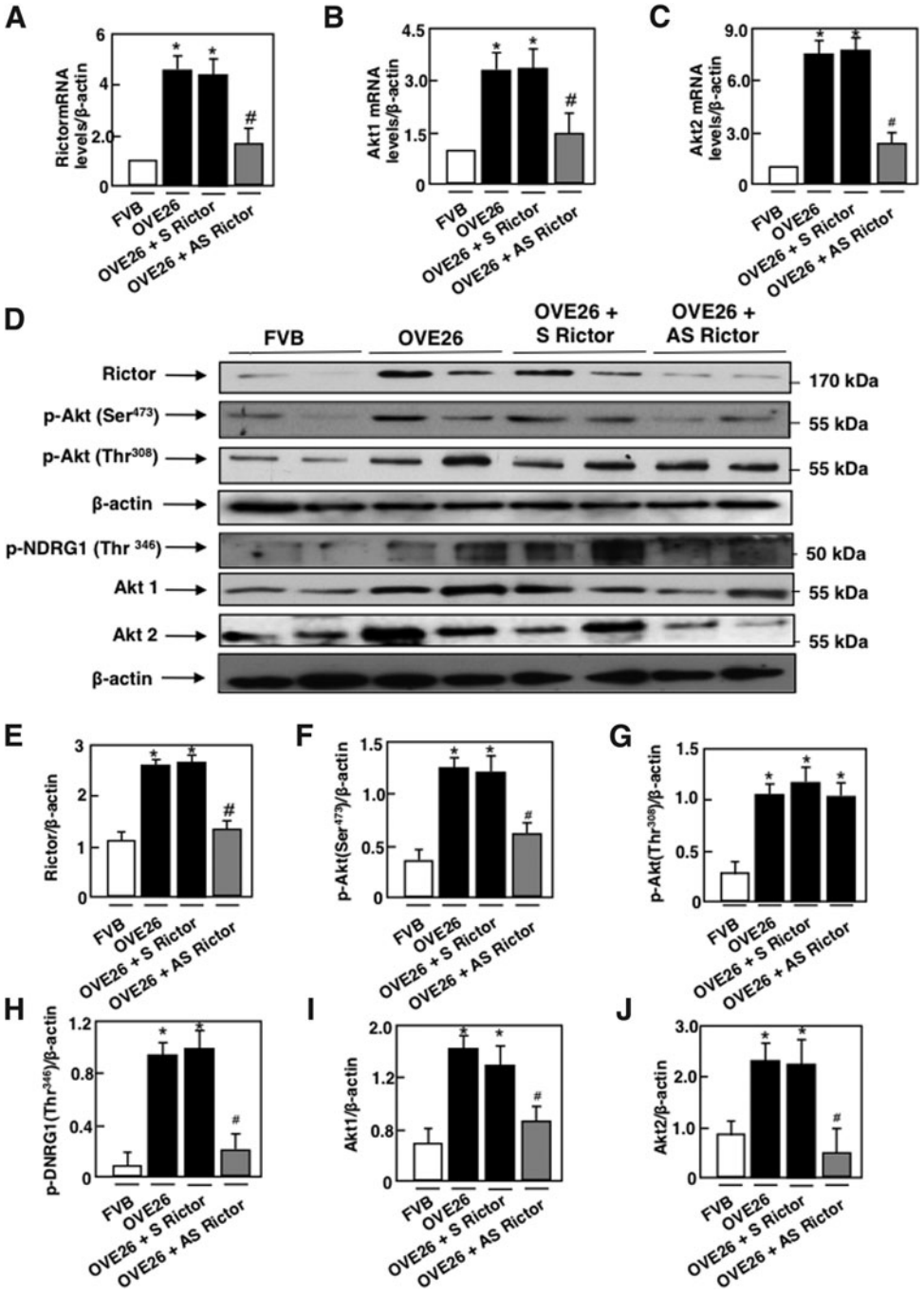

FIG. 5. Rictor/mTORC2 is activated in type 1 diabetes. OVE26 mice (17 weeks old) were treated with phosphorothioated sense (S) or AS oligonucleotides for Rictor (90 ng·g body $wt^{-1}\cdot day^{-1}$), administered subcutaneously by an ALZET osmotic minipump for 1 month. Mice in the control groups received saline vehicle also administered subcutaneously by an ALZET osmotic minipump. Glomeruli were isolated from the kidneys of the four groups of mice ($n=5$): group 1, FVB control mice; group 2, OVE26 mice; and groups 3 and 4, OVE26 mice treated with either S or AS. **(A)** Relative mRNA levels of Rictor. **(B)** Relative mRNA levels of Akt1. **(C)** Relative mRNA levels of Akt2. **(D)** Representative Western blot of Rictor, phospho-Ser^{473} Akt, phospho-Thr^{308} Akt, phospho-Thr^{346} NDRG1, Akt1, Akt2, and β-actin. β-actin was included as a control for loading and the specificity of change in protein expression. **(E)** Histograms showing quantitation of Rictor/β-actin from five different mice in each group. **(F)** Histograms showing quantitation of p-Akt (Ser473)/β-actin results from five different mice in each group. **(G)** Histograms showing quantitation of p-Akt (Thr308)/β-actin results from five different mice in each group. **(H)** Histograms showing quantitation of p-NDRG1 (Thr346)/β-actin results from five different mice in each group. **(I)** Histograms showing quantitation of Akt1/β-actin results from five different mice in each group. **(J)** Histograms showing quantitation of Akt2/β-actin results from five different mice in each group. **(K)** Representative Western blot of Raptor, phospho-Thr^{389} p70S6K, p70S6K, and β-actin. **(L)** Histograms showing quantitation of Raptor/β-actin results from five different mice in each group. **(M)** Histograms showing quantitation of p-p70S6KThr389/p70S6K results from five different mice in each group. Values are mean ± SE of five different animals from each group. $^{*}p<0.05$ *versus* vehicle-treated FVB mice; $^{\#}p<0.05$ *versus* vehicle-treated OVE26 mice. AS, antisense.

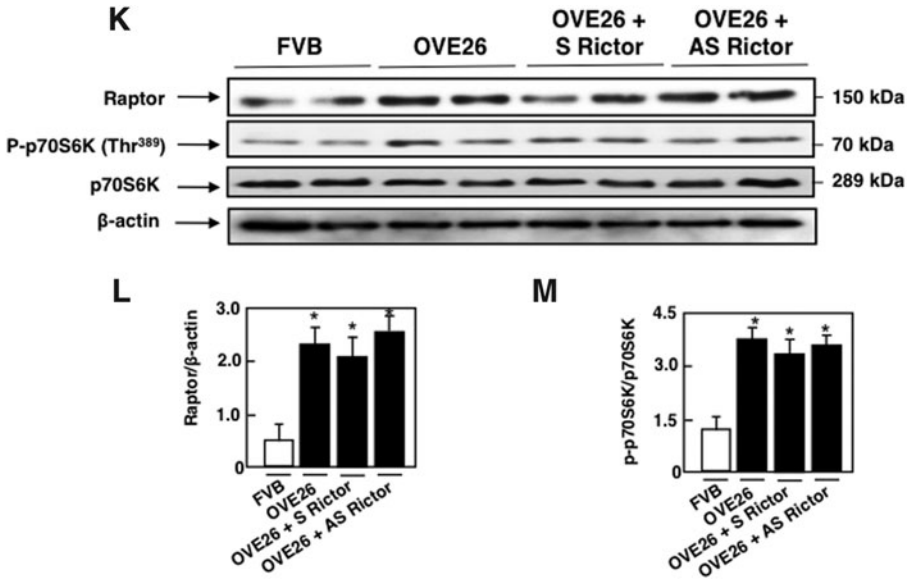

FIG. 5. (continued).

Rictor/mTORC2 pathway in OVE26 type 1 diabetic mice. As expected, levels of Nox4 mRNA and protein expression as well as NADPH oxidase activity and superoxide production were increased in glomeruli of OVE26 mice, an effect inhibited by AS treatment but not by S treatment (Fig. 6A–E).

Rictor/mTORC2 pathway regulates GBM thickening, foot process effacement, podocyte depletion, and albuminuria

Electron microscopic analysis revealed a significant increase in GBM thickening in the OVE26 mice compared to their control littermates, (Fig. 7A, B), paralleled by a marked effacement of foot processes (Fig. 7A, C). OVE26 diabetic mice lost podocytes, as assessed by the number of podocin-positive cells (Fig. 7D, E) and TUNEL-positive cells in the isolated glomeruli (Fig. 7F). Importantly, AS treatment resulted in a significant reversal of these glomerular changes (Fig. 7A–F) and decreased albuminuria (Fig. 7G). Sense treatment did not show any effect on diabetes-induced podocyte injury and enhanced albuminuria (Fig. 7A–G). Collectively, our *in vivo* results show that in type 1 OVE26 diabetic mice, Rictor/mTORC2 activation plays a key role in enhancing Nox4 expression and NADPH oxidase activity and highly contributes to glomerular cell injury and albuminuria (Figs. 6–8).

Discussion

Albuminuria/proteinuria is considered to be one of the most important risk factors for glomerulosclerosis and progressive renal fibrosis. The mechanisms leading to albuminuria in diabetes are not completely identified. There is increasing evidence that glomerular cell injury, including apoptosis, contributes to albuminuria and progressive glomerulosclerosis (16–19, 51). In this study, we provide evidence that podocyte depletion is mediated, at least partially, by the activation of the Rictor/mTORC2 pathway, enhanced NADPH oxidase, and upregulation of Nox4 leading to increased ROS generation. Furthermore, we show that this proapoptotic pathway is altered in glomeruli of the OVE26 type 1 diabetic mice. Inhibition of Rictor/mTORC2 axes in diabetic mice by the administration of AS oligonucleotides targeting Rictor attenuates Nox4 expression, NADPH oxidase activity, foot process effacement, GBM thickening, podocyte depletion, and albuminuria, without affecting the mTORC1-signaling pathway.

mTORC1 has been implicated in a number of biological responses (9, 16, 55), and its activation is controlled by tuberin, acting as a suppressor of mTORC1. We and others have previously shown that in the glomeruli of diabetic animals, the mTORC1/p70 S6Kinase pathway is activated, whereas tuberin is inactivated, contributing to matrix accumulation, GBM thickening, foot process effacement, and podocyte loss/apoptosis (16, 26, 30, 43). Moreover, activation of the mTORC1 in this system by inhibiting an upstream negative regulator hamartin (TSC1) recapitulated many features of DN, including podocyte loss, GBM thickening, mesangial expansion, and proteinuria in nondiabetic young and adult mice (26, 30, 47, 52). Furthermore, mTORC2 has been described to play a major role in diverse biological processes, including cell survival, metabolism, proliferation, and cytoskeletal organization (26, 30, 47, 52). In contrast to mTORC1, very little is known about mTORC2 function in renal epithelial physiology and pathophysiology. In fact, the role of mTORC2 in kidney epithelial biology has been controversial with paradoxical results provided by different studies (5, 26). For example, mTORC2 was described to play a key role in normal podocyte development (26). In addition, knocking down mTORC2 in mice sensitized them toward several injury models such as bovine serum albumin (BSA) overload indicating a major role for mTORC2 in podocyte stress surveillance and survival (26). Consistent with these observations, Canaud *et al.* showed that in chronic kidney disease, mTORC2 and its downstream target Akt2 maintain the function of podocytes and promote their survival and proliferation, while inactivation of mTORC2/Akt2 pathway resulted in podocyte apoptosis (5). In contrast, podocyte injury has been associated with an increase in the expression of

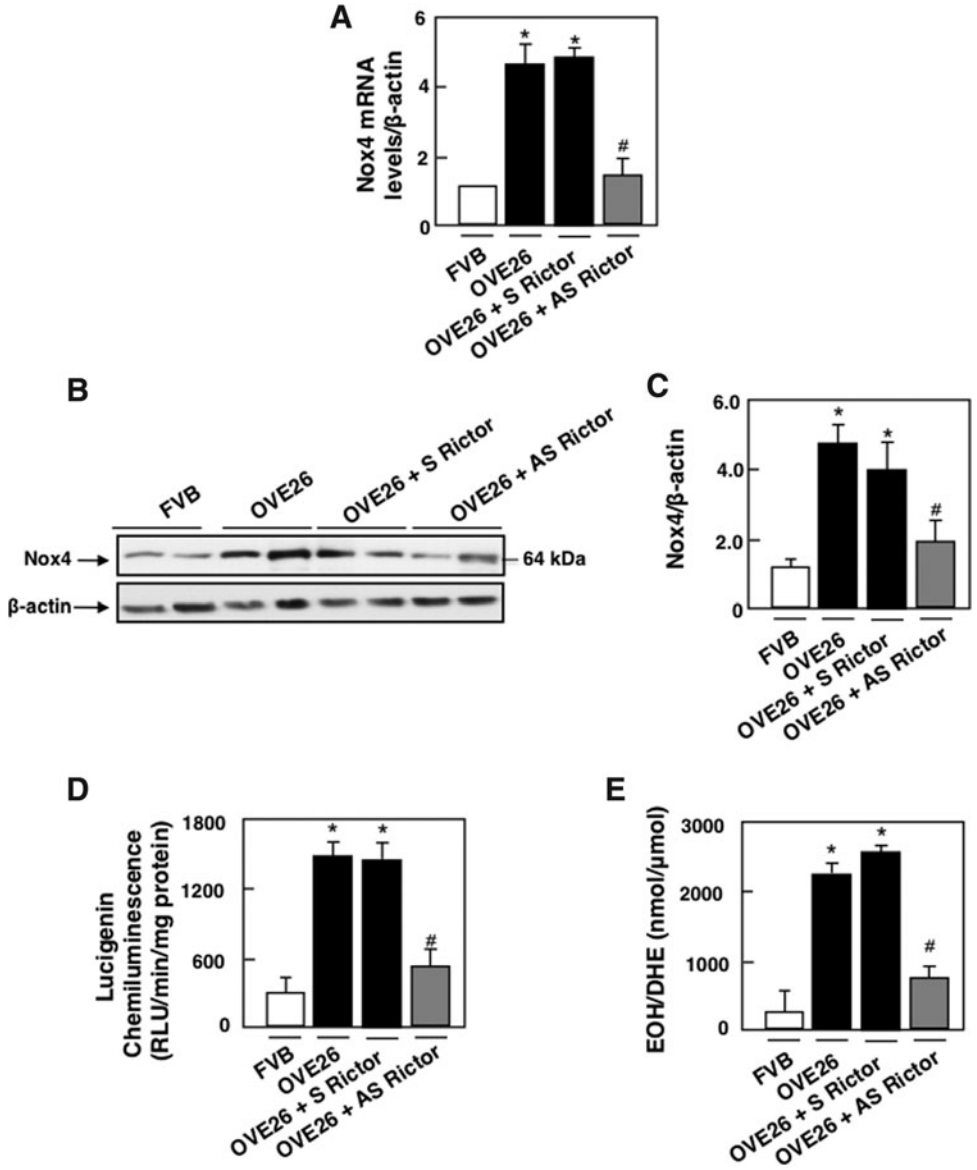

FIG. 6. Rictor/mTORC2 activation upregulates Nox4 and enhances NADPH oxidase activity and superoxide production in type 1 diabetes. OVE26 mice (17 weeks old) were treated with phosphorothioated sense (S) or AS oligonucleotides for Rictor (90 ng · g body wt^{-1} · day^{-1}), administered subcutaneously by an ALZET osmotic minipump for 1 month. Mice in the control groups received saline vehicle also administered subcutaneously by an ALZET osmotic minipump. Glomeruli were isolated from the kidneys of the four groups of mice ($n = 5$): FVB control mice, OVE26 mice, and OVE26 mice treated with either S or AS. **(A)** Relative mRNA levels of Nox4 in control FVB mice treated with vehicle, OVE26 mice treated with vehicle, and OVE26 mice treated either with S or AS. **(B)** Representative Western blot of Nox4 and β-actin levels. **(C)** Histograms showing Nox4/β-actin quantitation of results from five mice in the different groups. **(D)** NADPH-dependent superoxide generation. **(E)** Superoxide generation evaluated using DHE and HPLC. All values are mean ± SE of five different animals from each group. $^{*}p < 0.05$ *versus* vehicle-treated FVB mice; $^{\#}p < 0.05$ *versus* vehicle-treated OVE26 mice.

transient receptor potential cation channel 6 (TRPC6) (14). mTORC2 positively regulated TRPC6 in podocyte resulting in a massive calcium influx, which disrupted the filtration barrier, promoted the rearrangement of the highly dynamic podocyte actin cytoskeleton, and induced proteinuria. Inactivation of the Rictor/mTORC2 axis suppressed TRPC6 expression and decreased Ca^{+} influx into the podocytes, thus reducing injury (14). In line with the latter observation, we demonstrated that HG/hyperglycemia is associated with activation of the Rictor/mTORC2 signaling pathway and resulted in podocyte injury as assessed by a decrease in podocin expression and induction of podocyte loss/apoptosis. Inactivating the Rictor/mTORC2 pathway using AS oligonucleotide against Rictor inhibited HG- and hyperglycemia-induced alteration in podocin expression, podocyte apoptosis/loss, GBM thickening, foot process effacement, and more importantly produced a decrease in albuminuria. Also, our results show that Rictor inhibition was sufficient to reduce Akt phosphorylation on its hydrophobic motif site Ser473 by 60%–70%, as well as the phosphorylation of NDRG1 on its activating site Thr346, which is often used as

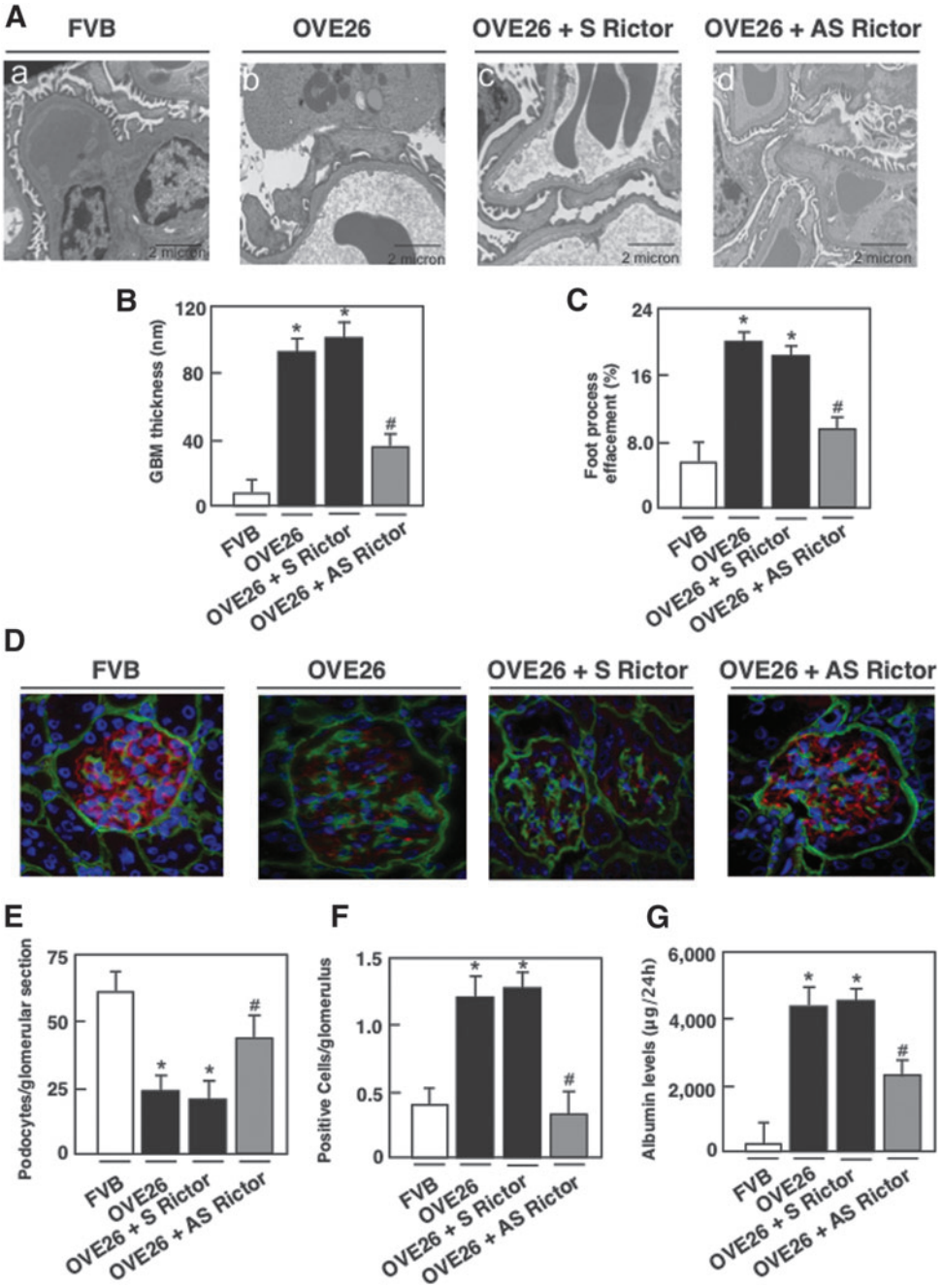

FIG. 7. Rictor/mTORC2 signaling regulates GBM thickening, foot process effacement, podocyte loss/apoptosis, and albuminuria in type 1 diabetic mice. OVE26 mice (17 weeks old) were treated with phosphorothioated sense (S) or AS oligonucleotides for Rictor (90 ng·g body $wt^{-1}\cdot day^{-1}$), administered subcutaneously by an ALZET osmotic minipump for 1 month. Mice in the control groups received saline vehicle also administered subcutaneously by an ALZET osmotic minipump. Glomeruli were isolated from the kidneys of the four groups of mice ($n=5$): FVB control mice, OVE26 mice, and OVE26 mice treated with either S or AS. **(A)** Representative transmission electron photomicrographs of glomerular cross section of FVB, OVE26, and OVE26 mice treated with either S or AS. The images show foot process effacement (*panel b*) and GBM (*panel b*) of an OVE26 mouse. This effect was not seen in the OVE26 mice treated with AS (*panel d*), while S did not reverse the effect of hyperglycemia seen in the OVE26 mice. **(B)** Histograms representing thickness of the GBM measured in nm and **(C)** semiquantitative analysis of foot process effacement of glomeruli from each group of animals. **(D)** Representative immunofluorescence images of glomeruli stained with collagen IV (*green*), podocin (*red*), and 4′,6-diamidino-2-phenylindole (*blue*). **(E)** Histogram representing podocyte number per glomerular section. Twenty-five to 35 glomeruli per mouse are counted. **(F)** Kidney sections of FVB, OVE26, and OVE26 mice treated with S and AS stained by TUNEL were quantified and total number of TUNEL-positive cells was reported in each group of mice. **(G)** FVB, OVE26, and OVE26 mice treated with either S or AS were placed in metabolic cages for 24 h, urine was collected, and albumin levels were measured. Values are mean ± SE. $^{*}p<0.05$ *versus* control FVB mice treated with vehicle; $^{\#}p<0.05$ *versus* OVE26 mice treated with vehicle ($n=5$ per group). GBM, glomerular basement membrane.

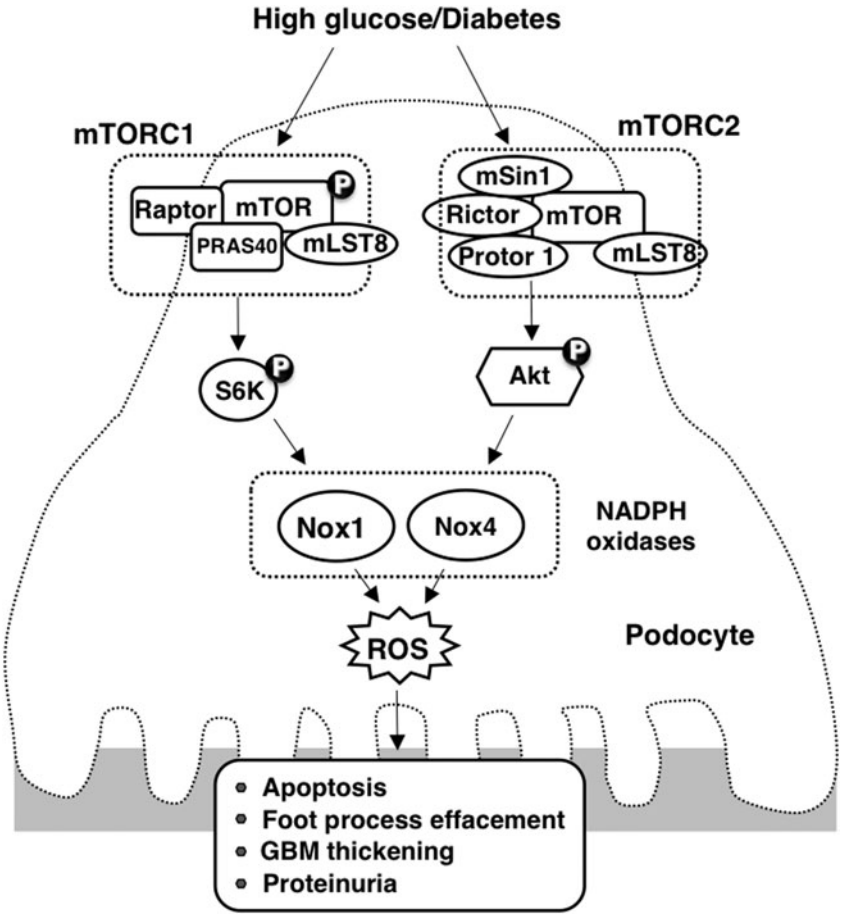

FIG. 8. Proposed mechanism of HG/diabetes-induced glomerular epithelial cell (podocyte) depletion/apoptosis.

a measure of mTORC2 activity. Concomitant with these observations, HG/hyperglycemia-induced Akt1 and Akt2 mRNA levels and protein expression were reversed with the use of siRictor. Taken together, these results implicate mTORC2 in the podocyte injury. It should be emphasized that our results show that the alteration in mRNA levels of Akt2, as well as Akt2 protein expression, is more projected then Akt1 mRNA levels and protein expression changes seen in the diabetic milieu. These later results can be explained by the fact that Akt2 is predominantly present in the podocytes (53). The use of siRictor reduced HG-induced phosphorylation of the mTORC 2 downstream effectors Akt^{Ser473} and $NDRG1^{Thr346}$ despite normal PDK1-dependent phosphorylation of Akt at T308. These results are in agreement with other Rictor knockout models, where activation of the T308 site is not altered (35, 42), suggesting that Rictor/mTORC2 mediates full Akt activation.

In this study, we have also denoted that Rictor/mTORC2 signaling pathway activation promoted podocyte injury independent of mTORC1 signaling, since HG in culture and hyperglycemia in OVE26 type 1 diabetic animals induced both mTORC1 and mTORC2 signaling. However, Rictor/mTORC2 activation contributed to HG- or hyperglycemia-induced podocyte injury independently of mTORC1 activation. Our previous published data (16) and our current findings underline the role of HG *in vitro* and hyperglycemia *in vivo* in inducing podocyte injury by activating mTORC1/p70S6kinase pathway (16) and/or mTORC2/Akt pathway. Blocking one of these pathways could partially reverse HG/hyperglycemia-induced glomerular injury, while blocking both pathways simultaneously reversed podocyte apoptosis to levels similar to control podocytes. It could be concluded that both signaling pathways contributed synergistically to the observed injury.

Oxidative stress, particularly ROS derived from the NAD(P)H oxidases Noxs, is crucial for the pathogenesis of diabetic kidney disease (4, 16–22, 29). The most abundant Nox isoform in the kidneys is Nox4 (3, 24, 25, 28). Nox4 was cloned from the renal system and is highly expressed in the tubules, renal fibroblasts, and cells of the glomerulus (18, 24, 28, 29). We have previously shown that podocyte exposed to HG treatment expressed an increase in Nox1 and Nox4 mRNA levels and protein expression, while Nox2 was not affected by the treatment (16–18). Impairment of Nox4 function using knockdown strategy in a diabetic milieu significantly reduces HG-induced podocyte apoptosis to levels almost similar to controls (16). Gray *et al.* (31) showed that Nox1 isoform is majorly implicated in diabetic macrovascular complications. Furthermore, in another recent study by Jha *et al.* (37), the authors show that albuminuria levels and urinary albumin/creatinine ratio are unaffected in diabetic $Nox1^{-/y}ApoE^{-/-}$ mice, while it was significantly reduced in diabetic $Nox4^{-/-}$ $ApoE^{-/-}$ when compared to diabetic wild-type controls. These findings suggest a major role played by Nox4 in diabetic renal injuries.

In our previous work, we show that mTORC1 positively regulates Nox4 mRNA levels and protein expression (19). In the current study, we demonstrate that mTORC2 inhibition decreases Nox1 and Nox4 expression and attenuates

HG-induced NADPH oxidase activity. Thus, our findings have established a previously unrecognized link between the Rictor/mTORC2 pathway and Nox1 and Nox4 in HG-induced podocyte loss and glomerular cell injury in cultured cells and in animal models of diabetes. Interestingly, there is evidence that NAD(P)H oxidase and/or ROS may also act upstream of Rictor/mTORC2 (27, 45), suggesting that ROS generated by mTORC2-induced Nox1 and/or Nox4 may target Rictor/mTORC2 activation *via* a feedback loop. In summary, to our knowledge, this is the first study to suggest that mTORC2 signaling regulates Nox1- and Nox4-induced podocyte depletion in DN.

Materials and Methods

Podocyte culture and transfection

Conditionally immortalized mouse podocytes, kindly provided by Dr. Katalin Susztack (Perelman School of Medicine, Philadelphia, PA), were cultured as described previously (16–19). For the siRNA experiments, SMART pool consisting of siRNA duplexes specific for mouse Rictor, or Raptor or Nox4, obtained from Dharmacon (Lafayette, CO). The SMART pool of siRNAs was introduced into the cells by the double transfection method using Oligofectamine or Lipofectamine 2000 as we have previously described (11, 12). The siRNAs were used at a concentration of 100 n*M*. Scrambled siRNAs (nontargeting siRNAs; 100 n*M*) served as controls to validate the specificity of the siRNAs. All incubations with HG were performed in the serum-free RPMI 1640 medium containing 0.2% BSA (fatty acid free) at 37°C for 24 or 48 h.

Animal models

All animal procedures were conducted in accordance with the University of Texas Health Science Center at San Antonio and the American University of Beirut Animal Care and Use Committee guidelines. Twenty-two-week-old control FVB mice and OVE26 mice (FVB background; The Jackson Laboratory) were used. At 17 weeks of age, OVE26 mice were treated by either phosphorothioated sense or AS oligonucleotides for Rictor ($90\,ng \cdot g$ body $wt^{-1} \cdot day^{-1}$) administered subcutaneously by an ALZET osmotic minipump (Alza). AS and the corresponding sense oligonucleotides were synthesized as phosphorothioated oligonucleotides and purified by HPLC (19). Glycemia levels (LifeScan One Touch Glucometer; Johnson & Johnson) were monitored 24 h after the treatment and then checked biweekly till the mice were sacrificed (50). All of the mice had unrestricted access to food and water and were maintained in accordance with protocols approved by the Institutional Animal Care and Use Committee. Before treatment with S or AS, mice were placed in metabolic cages for urine collection. Urine albumin was measured using a mouse albumin enzyme-linked immunosorbent assay (ELISA) quantification kit (Bethyl Laboratories) and expressed as micrograms of albumin/24 h. Animals were killed by exsanguination under anesthesia. Both kidneys were removed and weighed. A slice of kidney cortex at the pole was embedded in paraffin or flash-frozen in liquid nitrogen for microscopy and image analyses. Cortical tissues from the two kidneys of each mouse were used for isolation of glomeruli by differential sieving with minor modifications as described previously (16–19, 21, 22). Western blot analysis was performed on these isolated glomeruli.

Western blot analysis

Homogenates from glomeruli isolated from the renal cortex were prepared in 200 μl of radioimmunoprecipitation assay buffer (20 m*M* Tris-HCl [pH 7.5], 150 m*M* NaCl, 5 m*M* EDTA, 1 m*M* Na_3VO_4, 1 m*M* phenylmethylsulfonyl fluoride, 20 μg/ml aprotinin, 20 μg/ml leupeptin, and 1% Nonidet P-40) using a Dounce homogenizer. Homogenates were incubated for 1 h at 4°C and centrifuged at $10{,}000 \times g$ for 30 min at 4°C. Podocytes were lysed in radioimmunoprecipitation assay buffer at 4°C for 30 min. The cell lysates were centrifuged at $10{,}000 \times g$ for 30 min at 4°C. Protein in the supernatants was measured using the Bio-Rad method. For immunoblotting, proteins (30–60 μg) were separated by 12.5% sodium dodecyl sulfate–polyacrylamide gel electrophoresis and transferred to polyvinylidene difluoride membranes. The membranes were blocked with 5% low-fat milk in Tris-buffered saline and then incubated with the rabbit polyclonal Rictor antibody (dilution 1:1000; catalog No. 2140; Cell Signaling Technology, Inc.), rabbit polyclonal Raptor antibody (dilution 1:1000; catalog No. 4978; Cell Signaling Technology, Inc.), rabbit polyclonal phospho-Akt (Ser^{473}) antibody (dilution 1:1000; catalog No. 9271; Cell Signaling Technology, Inc.), rabbit polyclonal phospho-Akt (Thr^{308}) antibody (dilution 1:1000; catalog No. 9275; Cell Signaling Technology, Inc.), rabbit polyclonal Akt1 antibody (dilution 1:1500; catalog No. ab28422; Abcam), rabbit polyclonal Akt2 antibody (dilution 1:500; catalog No. PA5-13762; Thermo Fisher Scientific), rabbit polyclonal phospho-NDRG1 (Thr^{346}) antibody (dilution 1:1000; catalog No. PA5-17064; Thermo Fisher Scientific), rabbit polyclonal podocin antibody (1:300; catalog No. H-130; Santa Cruz Biotechnology, Inc.), rabbit polyclonal Mox1 antibody (1:300; catalog No. H-15; Santa Cruz Biotechnology, Inc.), rabbit polyclonal Nox4 antibody (1:300; catalog No. H-300; Santa Cruz Biotechnology, Inc.), rabbit polyclonal phospho-p70S6 Kinase (Thr^{389}) antibody (dilution 1:1000; catalog No. 9205; Cell Signaling Technology, Inc.), rabbit polyclonal p70S6 Kinase antibody (dilution 1:1000; catalog No. 9202; Cell Signaling Technology, Inc.), and mouse monoclonal anti-β-actin antibody (1:4000; catalog No. A2066; Sigma). The primary antibodies were detected using horseradish peroxidase-conjugated IgG (1:2500 or 1:5000). Bands were visualized by enhanced chemiluminescence. Densitometric analysis was performed using NIH Image software (16–19, 21, 22).

mRNA analysis

mRNA was analyzed by real-time RT-PCR using the $\Delta\Delta C_t$ method (9–14). Total RNA was isolated from cultured mouse podocytes or isolated glomeruli using the RNeasy® minikit (Qiagen, Valencia, CA). mRNA expression was quantified using the CFX96 Touch (Bio-Rad, Hercules, CA) with SYBR Green dye and predesigned mouse RT^2-quantitative PCR primers (SABiosciences, Frederick, MD) for Nox4 (RefSeq ID NM_015760), Rictor (RefSeq ID NM_030168), Akt1 (RefSeq ID NM_009652), Akt2 (RefSeq ID NM_007434), and normalized to β-actin (RefSeq ID NM_007393).

NADPH oxidase activity

NADPH oxidase activity was measured in cultured podocytes or in glomeruli isolated from kidney cortex as we have described previously (16–19, 21, 22). Cultured podocytes were washed five times with ice-cold phosphate-buffered saline and scraped from the plate in the same solution, followed by centrifugation at $800 \times g$ for 10 min at 4°C. The cell pellets were resuspended in lysis buffer (20 m*M* KH_2PO_4 [pH 7.0], 1 m*M* EGTA, 1 m*M* phenylmethylsulfonyl fluoride, 10 μg/ml aprotinin, and 0.5 μg/ml leupeptin). Cell suspensions or washed glomeruli were homogenized with 100 strokes in a Dounce homogenizer on ice. To start the assay, 20 μg of homogenates was added to 50 m*M* phosphate buffer (pH 7.0) containing 1 m*M* EGTA, 150 m*M* sucrose, 5 μM lucigenin, and 100 μM NADPH. Photon emission expressed as relative light units was measured every 20 or 30 s for 10 min in a luminometer. A buffer blank (<5% of the cell signal) was subtracted from each reading. The lucigenin-enhanced chemiluminescence assay is a reasonably good indicator of Nox4 capacity to generate superoxide indirectly when the probe is used at low concentrations (>20 μM) to avoid artifactual events (28). Superoxide production was expressed as relative light units/min/mg of protein. Protein content was measured using the Bio-Rad protein assay reagent.

Detection of intracellular superoxide in podocytes using HPLC

Cellular superoxide production in podocytes was assessed by HPLC analysis of DHE-derived oxidation products, as described previously (19, 28). The HPLC-based assay allows separation of superoxide-specific EOH from the nonspecific ethidium, as previously described (19, 28). Briefly, after exposure of quiescent podocytes grown in 60-mm dishes to 5 or 25 m*M* D-glucose for 48 h, cells are washed twice with Hanks' balanced salt solution (HBSS)-diethylenetriaminepentaacetic acid (DTPA) and incubated for 30 min with 50 μM DHE (Sigma-Aldrich) in HBSS–100 μM DTPA. Cells were harvested in acetonitrile and centrifuged ($12{,}000 \times g$ for 10 min at 4°C). The homogenate was dried under vacuum and analyzed by HPLC with fluorescence detectors. Quantification of DHE, EOH, and ethidium concentrations was performed by comparison of integrated peak areas between the obtained and standard curves of each product under chromatographic conditions identical to those described above. EOH and ethidium were monitored by fluorescence detection with excitation at 510 nm and emission at 595 nm, whereas DHE was monitored by ultraviolet absorption at 370 nm. The results are expressed as the amount of EOH produced (nmol) normalized for the amount of DHE consumed (*i.e.*, initial minus remaining DHE in the sample; μmol).

AMPK activity assay

AMPK activity was measured using AMPK KinEASE FP Fluorescein Green Assay Fluorescence Polarization according to the manufacturer's protocol (Millipore) (16, 17).

Apoptosis assays: cellular DNA fragmentation

The cellular DNA fragmentation ELISA (Roche Diagnostics GmbH, Mannheim, Germany) for detection of BrdU-labeled DNA fragments in culture supernatants and cell lysates was used according to the manufacturer's protocol (16–19, 21, 22).

Apoptosis assays: annexin V and propidium iodide staining

An Annexin V-FITC Apoptosis Detection Kit (Calbiochem) was used for annexin V and propidium iodide staining according to the manufacturer's protocol. The percentage of apoptotic and necrotic cells was assessed by FACS (16–19, 21, 22).

Apoptosis assays and caspase-3 activity

A Caspase-3 Fluorescence Assay Kit (Cayman Chemical Co.) was used according to the manufacturer's protocol (16–19, 21, 22).

TUNEL assay

TUNEL staining using the TUNEL Apoptosis Detection Kit (Upstate) was performed according to the manufacturer's instructions. The number of TUNEL-positive cells was counted in 25 randomly selected glomeruli (original magnification $\times 400$) for each animal (16). Five animals were studied per group ($n = 5$).

Podocyte enumeration

Dual-label immunohistochemistry was used to identify and count glomerular epithelial cells relative to the GBM as we previously described (16–19). To identify podocytes, 3-μm frozen sections of kidney cortex on glass slides were stained with anti-podocin antibody, followed by Cy3-labeled donkey anti-goat IgG. After washing and to identify the GBM, the sections were stained with a rabbit antibody directed against collagen type IV, followed by FITC-labeled donkey anti-rabbit IgG. After staining and washing, the sections were preserved on coverslips in the Prolong® gold antifade mounting medium with DAPI (Invitrogen) for fluorescence detection of nuclei. Sections were examined by epifluorescence using excitation and band-pass filters optimal for FITC, Cy3, and DAPI. Digital images representing each fluorochrome were taken of random glomeruli using a Zeiss LSM710 laser-scanning confocal microscope. Twenty-five to 35 glomerular cross sections per animal were photographed in each color channel, providing a minimum of 100 composite images per experimental group. Podocytes were counted in projected images in a blind manner by two individuals. Podocin-positive cells on the outer aspect of the GBM were considered glomerular epithelial cells and counted. Podocin-negative cells or cells in the inner aspect of the GBM were not counted. The mean area of each glomerular profile was measured manually, tracing the glomerular outline, encircling the area of interest, and calculating the surface area by computerized morphometry using MetaMorph (16–19, 23, 40, 49).

Electron microscopy

For electron microscopy photomicrographs, the kidney cortex was prepared and analyzed as we have previously described (16–19). In summary, the kidney cortex was cut into 0.5–1-mm^3 pieces and fixed overnight in cold 4%

formaldehyde and 1% glutaraldehyde in phosphate buffer and then embedded in Epon 812 resin. Plastic sections (0.50 mm) were cut and stained with toluidine blue for identification of representative areas for subsequent sectioning using an ultramicrotome. Ultrathin sections were stained with uranyl acetate and examined and photographed on a JEOL 100CX electron microscope. All electron microscopy photomicrographs were examined in a blind manner. Individual capillary loops were examined and quantified in five glomeruli/group of animals for the degree of foot process effacement as described by Jo *et al.* (38). The procedure adopted for GBM thickening measurement was a modification of the harmonic mean method summarized by Dische (15) and adapted from Jensen *et al.* (36) and Hirose *et al.* (32) as described in detail by Carlson *et al.* (6).

Statistical analysis

Results are expressed as mean ± standard error. Statistical significance was assessed by the analysis of variance and Student's *t*-test with Prism 6 software (GraphPad Software). Significance was determined as a probability (p value) of <0.05 (16–19, 21, 22).

Acknowledgments

This article is dedicated to the memory of a great friend and mentor Dr. H.E.A. Support for these studies was provided by the following sources: a regular research grant from the National Council for Scientific Research (Lebanon), a grant from the American University of Beirut, Faculty of Medicine MPP, a grant from the Qatar National Research Foundation (Doha, Qatar) (to A.A.E.), a grant from the Qatar National Research Foundation (Doha, Qatar) (to A.R. and A.H.). National Institute of Health grants UL1TR001120, RO1DK079996, and RO1DK033665 and a grant from Qatar National Research Foundation (Doha, Qatar) (to Y.G.), and a predoctoral fellowship grant from the National Council for Scientific Research (Lebanon) (to S.E.).

Author Disclosure Statement

No competing financial interests exist.

References

1. Abboud HE. Mesangial cell biology. *Exp Cell Res* 318: 979–985, 2012.
2. Alpers CE and Hudkins KL. Mouse models of diabetic nephropathy. *Curr Opin Nephrol Hypertens* 20: 278–284, 2011.
3. Bedard K and Krause KH. The NOX family of ROS-generating NADPH oxidases: Physiology and pathophysiology. *Physiol Rev* 87: 245–313, 2007.
4. Block K, Gorin Y, and Abboud HE. Subcellular localization of Nox4 and regulation in diabetes. *Proc Natl Acad Sci U S A* 106: 14385–14390, 2009.
5. Canaud G, Bienaimé F, Viau A, Treins C, Baron W, Nguyen C, Burtin M, Berissi S, Giannakakis K, Muda AO, Zschiedrich S, Huber TB, Friedlander G, Legendre C, Pontoglio M, Pende M, and Terzi F. AKT2 is essential to maintain podocyte viability and function during chronic kidney disease. *Nat Med* 19: 1288–1296, 2013.
6. Carlson EC, Audette JL, Klevay LM, Nguyen H, and Epstein PN. Ultrastructural and functional analyses of nephropathy in calmodulin-induced diabetic transgenic mice. *Anat Rec* 247: 9–19, 1997.
7. Clempus RE, Sorescu D, Dikalova AE, Pounkova L, Jo P, Sorescu GP, Schmidt HH, Lassegue B, and Griendling KK. Nox4 is required for maintenance of the differentiated vascular smooth muscle cell phenotype. *Arterioscler Thromb Vasc Biol* 27: 42–48, 2007.
8. Cucoranu I, Clempus R, Dikalova A, Phelan PJ, Ariyan S, Dikalov S, and Sorescu D. NAD(P)H oxidase 4 mediates transforming growth factor-beta1-induced differentiation of cardiac fibroblasts into myofibroblasts. *Circ Res* 97: 900–907, 2005.
9. Dann SG, Selvaraj A, and Thomas G. mTOR Complex1-S6K1 signaling: At the crossroads of obesity, diabetes and cancer. *Trends Mol Med* 13: 252–259, 2007.
10. Das F, Ghoch-Choudhury N, Bera A, Dey N, Abboud HE, Kasinath BS, and Choudhury GG. Transforming growth factor β integrates Smad 3 to mechanistic target of rapamycin complexes to arrest deptor abundance for glomerular mesangial cell hypertrophy. *J Biol Chem* 288: 7756–7768, 2013.
11. De Zeeuw D, Remuzzi G, Parving H, Keane W, Zhang Z, Shahinfar S, Snapinn S, Cooper M, Mitch W, and Brenner BM. Proteinuria, a target for renoprotection in patients with type 2 diabetic nephropathy: Lessons from RENAAL. *Kidney Int* 65: 2309–2320, 2004.
12. Dias N and Stein CA. Antisense oligonucleotides: Basic concepts and mechanisms. *Mol Cancer Ther* 1: 347–355, 2002.
13. Dikalov S, Griendling KK, and Harrison DG. Measurement of reactive oxygen species in cardiovascular studies. *Hypertension* 49: 717–727, 2007.
14. Ding F, Zhang X, Li X, Zhang Y, Li B, and Ding J. Mammalian target of rapamycin complex 2 signaling pathway regulates transient receptor potential cation channel 6 in podocytes. *PLoS One* 9: e112972, 2014.
15. Dische FE. Measurement of glomerular basement membrane thickness and its application to the diagnosis of thin-membrane nephropathy. *Arch Pathol Lab Med* 116: 43–49, 1992.
16. Eid AA, Ford BM, Bhandary B, Cavagliery R, Block K, Barnes JL, Gorin Y, Choudhury GG, and Abboud HE. mTOR regulates Nox4-mediated podocyte depletion in diabetic renal injury. *Diabetes* 62: 2935–2947, 2013.
17. Eid AA, Ford BM, Block K, Kasinath BS, Gorin Y, Ghosh-Choudhury G, Barnes JL, and Abboud HE. AMP-activated protein kinase (AMPK) negatively regulates Nox4-dependent activation of p53 and epithelial cell apoptosis in diabetes. *J Biol Chem* 285: 37503–37512, 2010.
18. Eid AA, Gorin Y, Fagg BM, Maalouf R, Barnes JL, Block K, and Abboud HE. Mechanisms of podocyte injury in diabetes: Role of cytochrome P450 and NADPH oxidases. *Diabetes* 58: 1201–1211, 2009.
19. Eid AA, Lee DY, Roman LJ, Khazim K, and Gorin Y. Sestrin 2 and AMPK connect hyperglycemia to Nox4-dependent endothelial nitric oxide synthase uncoupling and matrix protein expression. *Mol Cell Biol* 33: 3439–3460, 2013.
20. Eid S, Abdul-Massih C, El-Khuri CM, Hamdy A, Rashid A, and Eid AA. New mechanistic insights in the development of diabetic nephropathy: Role of cytochromes P450 and their metabolites. *J Endocr Disord* 1: 6, 2014.
21. Eid S, Abou-Kheir W, Sabra R, Daoud D, Jaffa A, Ziyadeh FN, Roman L, and Eid AA. Involvement of renal cytochromes P450 and arachidonic acid metabolites in diabetic

nephropathy. *J Biol Regul Homeost Agents* 27: 693–703, 2013.
22. Eid S, Maalouf R, Jaffa A, Nassif J, Ziyadeh FN, and Eid AA. 20-HETE and EETs in diabetic nephropathy: A novel mechanistic pathway. *PLoS One* 8: e70029, 2013.
23. Faulkner JL, Szcykalski LM, Springer F, and Barnes JL. Origin of interstitial fibroblasts in an accelerated model of angiotensin II-induced renal fibrosis. *Am J Pathol* 167: 1193–1205, 2005.
24. Geiszt M. NADPH oxidases: New kids on the block. *Cardiovasc Res* 71: 289–299, 2006.
25. Gill PS and Wilcox CS. NADPH oxidases in the kidney. *Antioxid Redox Signal* 8: 1597–1607, 2006.
26. Gödel M, Hartleben B, Herbach N, Liu S, Zschiedrich S, Lu S, Debreczeni-Mór A, Lindenmeyer MT, Rastaldi MP, Hartleben G, Wiech T, Fornoni A, Nelson RG, Kretzler M, Wanke R, Pavenstädt H, Kerjaschki D, Cohen CD, Hall MN, Rüegg MA, Inoki K, Walz G, and Huber TB. Role of mTOR in podocyte function and diabetic nephropathy in humans and mice. *J Clin Invest* 121: 2197–2209, 2011.
27. Goncharov DA, Kudryashova TV, Ziai H, Ihida-Stansbury K, DeLisser H, Krymskaya VP, Tuder RM, Kawut SM, and Goncharova EA. Mammalian target of rapamycin complex 2 (mTORC2) coordinates pulmonary artery smooth muscle cell metabolism, proliferation, and survival in pulmonary arterial hypertension. *Circulation* 129: 864–874, 2014.
28. Gorin Y and Block K. Nox4 and diabetic nephropathy: With a friend like this who needs enemies? *Free Radic Biol Med* 0: 130–142, 2013.
29. Gorin Y, Block K, Hernandez J, Bhandari B, Wagner B, Barnes JL, and Abboud HE. Nox4 NAD(P)H oxidase mediates hypertrophy and fibronectin expression in the diabetic kidney. *J Biol Chem* 280: 39616–39626, 2005.
30. Grahammer F, Wanner N, and Huber T. mTOR controls epithelia in health and diseases. *Nephrol Dial Transplant* 29: i9–i18, 2014.
31. Gray SP, Di Marco E, Okabe J, Szyndralewiez C, Heitz F, Montezano AC, de Haan JB, Koulis C, El-Osta A, Andrews KL, Chin-Dusting JP, Touyz RM, Wingler K, Cooper ME, Schmidt HH, and Jandeleit-Dahm KA. NADPH oxidase 1 plays a key role in diabetes mellitus-accelerated atherosclerosis. *Circulation* 127: 1888–1902, 2013.
32. Hirose K, Osterby R, Nozawa M, and Gundersen HJ. Development of glomerular lesions in experimental long-term diabetes in the rat. *Kidney Int* 21: 689–695, 1982.
33. Infanger DW, Cao X, Butler SD, Burmeister MA, Zhou Y, Stupinski JA, Sharma RV, and Davisson RL. Silencing nox4 in the paraventricular nucleus improves myocardial infarction-induced cardiac dysfunction by attenuating sympathoexcitation and periinfarct apoptosis. *Circ Res* 106: 1763–1774, 2010.
34. Inoki K, Mori H, Wang J, Suzuki T, Hong S, Yoshida S, Blattner SM, Ikenoue T, Rüegg MA, Hall MN, Kwiatkowski DJ, Rastaldi MP, Huber TB, Kretzler M, Holzman LB, Wiggins RC, and Guan KL. mTORC1 activation in podocytes is a critical step in the development of diabetic nephropathy in mice. *J Clin Invest* 121: 2181–2196, 2011.
35. Jacinto E, Facchinetti V, Liu D, Soto N, and Wei S. SIN1/MIP1 maintains rictor-mTOR complex integrity and regulates Akt phosphorylation and substrate specificity. *Cell* 127: 125–137, 2006.
36. Jensen EB, Gundersen HJ, and Osterby R. Determination of membrane thickness distribution from orthogonal intercepts. *J Microsc* 115: 19–33, 1979.
37. Jha JC, Gray SP, Barit D, Okabe J, El-Osta A, Namikoshi T, Thallas-Bonke V, Wingler K, Szyndralewiez C, Heitz F, Touyz RM, Cooper ME, Schmidt HHW, and KariJandeleit-Dahm KA. Genetic targeting or pharmacologic inhibition of NADPH oxidase Nox4 provides renoprotection in long-term diabetic nephropathy. *J Am Soc Nephrol* 25: 1237–1254, 2014.
38. Jo YI, Cheng H, Wang S, Moeckel GW, and Harris RC. Puromycin induces reversible proteinuric injury in transgenic mice expressing cyclooxygenase-2 in podocytes. *Nephron Exp Nephrol* 107: e87–e94, 2007.
39. Kanwar YS, Sun L, Xie P, Liu FY, and Chen S. A glimpse of various pathogenetic mechanisms of diabetic nephropathy. *Annu Rev Pathol* 6: 395–423, 2011.
40. Kim YH, Goyal M, Kurnit D, Wharram B, Wiggins J, Holzman L, Kershaw D, and Wiggins R. Podocyte depletion and glomerulosclerosis have a direct relationship in the PAN-treated rat. *Kidney Int* 60: 957–968, 2001.
41. Kleinschnitz C, Grund H, Wingler K, Armitage ME, Jones E, Mittal M, Barit D, Schwarz T, Geis C, Kraft P, Barthel K, Schuhmann MK, Herrmann AM, Meuth SG, Stoll G, Meurer S, Schrewe A, Becker L, Gailus-Durner V, Fuchs H, Klopstock T, de Angelis MH, Jandeleit-Dahm K, Shah AM, Weissmann N, and Schmidt HH. Post-stroke inhibition of induced NADPH oxidase type 4 prevents oxidative stress and neurodegeneration. *PLoS Biol* 8: pii:e1000479, 2010.
42. Kumar A, Harris TE, Keller SR, Choi KM, and Magnuson MA. Muscle-specific deletion of rictor impairs insulin-stimulated glucose transport and enhances Basal glycogen synthase activity. *Mol Cell Biol* 28: 61–70, 2008.
43. Laplante M and Sabatini DM. mTOR signaling at a glance. *J Cell Sci* 122: 3589–3594, 2009.
44. Meyer TW, Bennett PH, and Nelson RG. Podocyte number predicts long-term urinary albumin excretion in Pima Indians with type II diabetes and microalbuminuria. *Diabetologia* 42: 1341–1344, 1999.
45. Nayak BK, Feliers D, Sudarshan S, Friedrichs WE, Day RT, New DD, Fitzgerald JP, Eid A, Denapoli T, Parekh DJ, Gorin Y, and Block K. Stabilization of HIF-2α through redox regulation of mTORC2 activation and initiation of mRNA translation. *Oncogene* 32: 3147–3155, 2013.
46. Pagtalunan ME, Miller PL, Jumping-Eagle S, Nelson RG, Myers BD, Rennke HG, Coplon NS, Sun L, and Meyer TW. Podocyte loss and progressive glomerular injury in type II diabetes. *J Clin Invest* 99: 342–348, 1997.
47. Polak P and Hall MN. mTOR and the control of whole body metabolism. *Curr Opin Cell Biol* 21: 209–218, 2009.
48. Sabatini DM. mTOR and cancer: insights into a complex relationship. *Nat Rev Cancer* 6: 729–734, 2006.
49. Sanden SK, Wiggins JE, Goyal M, Riggs LK, and Wiggins RC. Evaluation of a thick and thin section method for estimation of podocyte number, glomerular volume, and glomerular volume per podocyte in rat kidney with Wilms' tumor-1 protein used as a podocyte nuclear marker. *J Am Soc Nephrol* 14: 2484–2493, 2003.
50. Sarbassov DD, Guertin DA, Ali SM, and Sabatini DM. Phosphorylation and regulation of Akt/PKB by the rictor-mTOR complex. *Science* 307: 1098–1101, 2005.
51. Susztak K, Raff AC, Schiffer M, and Böttinger EP. Glucose-induced reactive oxygen species cause apoptosis of podocytes and podocyte depletion at the onset of diabetic nephropathy. *Diabetes* 55: 225–233, 2006.
52. Torras J, Herrero-Fresneda I, Gulias O, Flaquer M, Vidal A, Cruzado JM, Lloberas N, Franquesa MI, and Grinyó JM. Rapamycin has dual opposing effects on proteinuric

experimental nephropathies: is it a matter of podocyte damage? *Nephrol Dial Transplant* 24: 3632–3640, 2009.
53. Tschopp O, Yang ZZ, Brodbeck D, Dummler BA, Hemmings-Mieszczak M, Watanabe T, Michaelis T, Frahm J, Hemmings BA. Essential role of protein kinase B gamma (PKB gamma/Akt3) in postnatal brain development but not in glucose homeostasis. *Development* 132: 2943–2954, 2005.
54. Um SH, D'Alessio D, and Thomas G. Nutrient overload, insulin resistance, and ribosomal protein S6 kinase 1, S6K1. *Cell Metab* 3: 393–402, 2006.
55. Vergès B and Cariou B. mTOR inhibitors and diabetes. *Diabetes Res Clin Pract* 110: 101–108, 2015.
56. Wullschleger S, Loewith R, and Hall MN. TOR signaling in growth and metabolism. *Cell* 124: 471–484, 2006.
57. Zheng S, Noonan WT, Metreveli NS, Coventry S, Kralik PM, Carlson EC, and Epstein PN. Development of late-stage diabetic nephropathy in OVE26 diabetic mice. *Diabetes* 53: 3248–3257, 2004.

Address correspondence to:
Dr. Assaad A. Eid
Faculty of Medicine and Medical Center
Department of Anatomy, Cell Biology and Physiological Sciences
American University of Beirut
PO Box 11-0236
Riad El-Solh 1107 2020
Beirut
Lebanon

E-mail: ae49@aub.edu.lb

Date of first submission to ARS Central, November 5, 2015; date of final revised submission, June 18, 2016; date of acceptance, June 20, 2016.

Abbreviations Used

4E-BP1 = eukaryotic initiation factor 4E binding protein 1
Akt = protein kinase B
AMPK = AMP-activated protein kinase
AS = antisense
BSA = bovine serum albumin
DHE = dihydroethidium
DN = diabetic nephropathy
DTPA = diethylenetriaminepentaacetic acid
ELISA = enzyme-linked immunosorbent assay
EOH = 2-hydroxyethidium
GBM = glomerular basement membrane
HBSS = Hanks' balanced salt solution
HG = high glucose
HPLC = high performance liquid chromatography
mLST8 = mammalian lethal with Sec13 protein 8
mRNA = messenger RNA
mTORC1 = mammalian target of rapamycin complex 1
mTORC2 = mammalian target of rapamycin complex 2
NADPH = nicotinamide adenine dinucleotide 3-phosphate
Nox1 = NADPH oxidase 1
Nox4 = NADPH oxidase 4
p70S6K = 70-kDa ribosomal protein S6 kinase
Raptor = regulatory-associated protein of mTOR
Rictor = rapamycin-insensitive companion of mTOR
ROS = reactive oxygen species
S = sense
Ser = serine
siRNA = small interfering RNA
Thr = threonine
TRPC6 = transient receptor potential cation channel 6
UFR = urine flow rate